JOURNAL OF SOLID STATE CHEMISTRY **121,** 430–436 (1996)
ARTICLE NO. 0059

Structure and Ionic Conductivity of $NaLnTiO_4$; Comparison with Those of $Na_2Ln_2Ti_3O_{10}$ (Ln = La, Nd, Sm, and Gd)

Song-Ho Byeon* and Kileung Park

Department of Chemistry, College of Natural Sciences, Kyung Hee University, Kyung Ki 449-701, Korea

and

Mitsuru Itoh

Research Laboratory of Engineering Materials, Tokyo Institute of Technology, 4259 Nagatsuta, Midori-ku, Yokohama 226, Japan

Received July 6, 1995; in revised form October 18, 1995; accepted October 29, 1995

The crystal structures of $NaLnTiO_4$ (Ln = La, Nd, Sm, and Gd) were determined by Rietveld refinements on their powder X-ray diffraction patterns. They had K_2NiF_4-type related superstructure (space group $P4/nmm(D_{4h}^7)$) in which NaO and LnO double layers are 1:1 ordered perpendicular to the c axis. Although the c parameter decreases from Ln = La to Nd, Sm, and Gd, the Na–O distance along the c axis was not proportional to the variation of the unit cell parameter. A strong corrugation of the LnO layer which is the main factor determining the a parameter was observed, which would be induced by the poor charge compensation between NaO and LnO layers. Due to such a corrugation, the a parameter did not show decreasing tendency despite the fact that the constituting lanthanide ion becomes smaller. Ionic conductivity of $NaLnTiO_4$ lower than that of $Na_2Ln_2Ti_3O_{10}$ (Ln = La, Nd, Sm, and Gd) also resulted from the corrugation of the LnO layer with coordination number 9 accompanied by contraction of the NaO layer.

INTRODUCTION

The perovskite-derived layered structures with general formule, $A'_2[A_{n-1}B_nO_{3n+1}]$ Ruddlesden-Popper phases (1) and $A'[A_{n-1}B_nO_{3n+1}]$ Dion–Jacobson phases (2, 3) where A' = alkali-metal cations, are two of the most intensively studied structure in recent times. These structures consist of two-dimensional perovskite slabs which are separated by A' layers perpendicular to the c axis. Particularly, $n = 2$ and 3 members for each series have attracted considerable attention for their possibilities to ion exchange, intercalation, and interlayer reactions in A' layers as well as the application as acid catalysts and photocatalysts (4–9).

Compared with $n = 2$ and 3 members, there have been few studies on $n = 1$ members that have layers consisting of alkali-metal cations. If we consider the $(A, A')_2$ $(M, M')O_4$ (A and A' = alkaline-earth or rare-earth cations) with tetragonal K_2NiF_4-type structure corresponding to $n = 1$ member of the Ruddlesden–Popper series, large A and A' ions are in general randomly distributed among the larger cation sites. Concerning small cations, a disordered arrangement of M and M' ions in the perovskite slab leads to $I4/mmm$ space group while a distribution with ordered manner results in $P422$ space group (10). The evidences for an 1:1 ordering of M and M' cations have been observed for several kinds of cationic pairs such as (Li, Mn), (Li, Fe), (Li, Co), (Li, Ni), (Mg, Mn), (Mg, Fe), (Mg, Co), (Mg, Ni), (Zn, Mn), (Zn, Fe), (Zn, Co), and (Zn, Ni) (11–16). The additional energies obtained by cationic ordering are about 10 ~ 11 kcal/ion (10). Due to the two-dimensional character of this structure, such an energy is smaller than those (14 ~ 15 kcal/ion) for the typical ordered perovskite structure. An important factor determining such an ordering have been proposed to be the difference in ionic radius between two cations (17). The ordering of anions in the K_2NiF_4-type structure has been also observed. If the unit cells of tetragonal K_2MgCl_4 and $K_2MgCl_2Br_2$ are compared, for example, the c parameter is considerably larger in the latter than in the former, whereas the a parameter is essentially constant. This indicated that the Cl^- ions occupy the sites in the base plane of the tetragonal unit cell while the Br^- ions are located in the sites on the c axis (18). The ordered distribution of A and A' caions along the c axis, however, is rare. As far as we know, $NaLnTiO_4$ (Ln = Y and lanthanides) prepared by Blasse (19) would be an unique example. From the observation of intense reflections with $h + k + l$ = odd, he has proposed that the Na^+ and Ln^{3+} ions be arranged in an ordered way without changing the dimensions of the unit cell. Similar

* To whom correspondence should be addressed.

0022-4596/96 $18.00

ordering of M^+ (M = Na and K) and La^{3+} cations has been also observed in the alkali-metal-doped lathanium copper oxides $La_{2-x}M_xCuO_4$ (20). Recently, however, a different structural model for $NaYTiO_4$ was suggested (21). In this model, every other perovskite slab is stacked without gliding by $\frac{1}{2}$ along the [110] direction and one NaCl-type layer is present in the interslab space.

During our studies (22) on the correlation between the structural variations and the ionic conductivities of $Na_2Ln_2Ti_3O_{10}$ (Ln = lanthanide cations), we became interested in NaLnTiO$_4$ when is an $n = 1$ member of the Ruddlesden–Popper series. This is because, if the NaO and LnO layers are 1 : 1 ordered in NaLnTiO$_4$, a considerable charge unbalance between the two layers would modify the local environment of the NaO layer differently from that in $Na_2Ln_2Ti_3O_{10}$. Such a modification would induce a different conduction behavior. In this work, the structural details of NaLnTiO$_4$ (Ln = La, Nd, Sm, and Gd) are refined by Rietveld analyses of their powder X-ray diffraction data. From the structural similarity and difference, the thermal behavior and the ionic conductivity of Na LnTiO$_4$ are discussed and compared with those of $Na_2Ln_2Ti_3O_{10}$.

EXPERIMENTALS

NaLnTiO$_4$ (Ln = La, Nd, Sm, and Gd) were prepared by conventional solid state reactions. The stoichiometric amounts of Ln_2O_3 and TiO_2 (anatase) and 20% excess of Na_2CO_3 were mixed, slowly heated up to 800°C (1°C/min.), and kept constant for 12 hours in air. Ln_2O_3 was preheated at 900°C for 12 hours, cooled to room temperature in desiccator, and directly weighed. The resulting powder was ground, heated at 900°C for 2 days with two intermittent grindings, and cooled in the furnace. Twenty percent excess of Na_2CO_3 was added on every grinding to compensate for the loss of the volatile sodium component. After the reaction, the products were washed with distilled water and dried at 120°C. For the specimens to measure ionic conductivity, the well-dried products were pressed into pellets and heated at 920°C for 5 hours. $Na_2Ln_2Ti_3O_{10}$ (Ln = La, Nd, Sm, and Gd) were prepared as previously described (22).

The sodium contents in the final products were determined by the inductively coupled plasma (ICP) method using the BAIRD ICP 2070 instrument. The obtained molar ratios of sodium per formula unit showed that the Na deficiencies could be neglected within experimental errors.

The thermogravimetric analysis (TGA) and differential thermal analysis (DTA) were carried out from room temperature to 1700 K (2 K/min heating rate) in air using TG/DTA320 Seico Instruments Inc.

Powder X-ray diffraction data for Rietveld refinements were recorded on a rotating anode installed M18XHFMAC Science diffractometer using Cu$K\alpha$ radiation monochromatized by the curved graphite. The data were collected with a step-scan procedure in the range $2\theta = 20°$ to 120° with counts for a second at 0.02° intervals. The fitting of reflection positions and intensities were carried out using Rietveld analysis program RIETAN (Macintosh version) (23).

Sodium ion conductivities of NaLnTiO$_4$ were measured on an Au-pasted pellet by a complex impedance technique between 5 Hz and 13 MHz using an HP4192A impedance analyzer in the temperature range of 300–1000 K.

TABLE 1
Sodium Contents in NaLnTiO$_4$ Determined by ICP

Compounds	Molar ratio of sodium per formular
$NaLaTiO_4$	0.99(1)
$NaNdTiO_4$	0.987(6)
$NaSmTiO_4$	0.983(4)
$NaGdTiO_4$	0.985(7)

RESULTS AND DISCUSSION

Synthesis and Thermal Behavior

At first, the preparations of the single-phase NaLnTiO$_4$ were tried at 1050°C as reported by Blasse. However, the final products always had several impurity phases, one of which corresponds to $Na_2Ln_2Ti_3O_{10}$. In fact, the formation of such impurities could not be avoided at temperature higher than 1000°C. On the other hand, well-crystallized single phases were obtained at the final temperature range of 900–950°C. Quantitative analyses by ICP revealed that a loss of volatile sodium at high temperature can be compensated for by an addition of excess Na_2CO_3 during preparation. The experimental sodium contents are listed in Table 1. The results of thermogravimetric analyses showed that NaLnTiO$_4$ is stable up to about 960°C and slowly decomposes from about 1000°C. For Ln = Nd, Sm, and Gd, $Ln_2Ti_2O_7$ pyrochlores were formed at around 1400°C whose structures could be confirmed by X-ray diffraction. For Ln = La, however, a single phase of $La_2Ti_2O_7$ was not formed but the mixture of pyrochlore, defective perovskite, and TiO_2 phases was obtained after heating up to 1400°C. Any significant weight change resulting from the loss of water molecules was not observed. The single phases of NaLnTiO$_4$ could be formed again when $Ln_2Ti_2O_7$ (Ln = Nd, Sm, and Gd) pyrochlores and the decomposed product of $NaLaTiO_4$ were reacted with Na_2CO_3 at 950°C for two days with two intermittent grindings and additions of excess Na_2CO_3.

Structure

Daoudi (24) had proposed that an ordering between Ca^{2+} and Ln^{3+} cations along the c axis in CaLnAlO$_4$ can

TABLE 2
Crystallographic Data for Na*Ln*TiO$_4$

	$NaLaTiO_4$	$NaNdTiO_4$	$NaSmTiO_4$	$NaGdTiO_4$
Space group	*P*4/*nmm*	*P*4/*nmm*	*P*4/*nmm*	*P*4/*nmm*
a (Å)	3.77343(4)	3.75055(4)	3.76127(4)	3.77085(7)
c (Å)	13.0178(1)	12.8242(1)	12.6335(2)	12.4644(2)
ρ(g/cm^3)	4.89	5.13	5.29	5.39
Bragg (R_I, %)	1.63	2.37	2.38	2.71
Weighted profile (R_{WP}, %)	9.69	10.07	11.16	9.90
Profile (R_P, %)	6.81	7.33	8.14	7.33
Expected (R_E, %)	6.34	4.67	4.94	4.77

be characterized by the occupation ratio of two cations in position 2a of space group *I*4mm (C_{4v}^9). The comparison of the observed intensities with those calculated indicated a disordered arrangement of Ca^{2+} and Ln^{3+} ions in the planes perpendicular to the *c* axis. At first, we applied this method to determine the distribution of Na^+ and Ln^{3+} ions. However, a large differences between calculated and observed intensities of 101, 112, 105, 202 reflection peaks as well as an existence of intense reflections with $h + k + l$ = odd in X-ray diffraction patterns suggested that Na^+ and Ln^{3+} ions would not form body-centered lattice. This phenomenon may result from strong displacement of the Ti^{4+} ion from the center of symmetry, which would be a consequence of poor charge compensation by an ordering of Na^+ and Ln^{3+} ions along the *c* axis. The refinements of the experimental intensity data, therefore, were carried out again on the basis of space group *P*4*mm* (C_{4v}^1) as proposed by Blasse and Van den Heuvel (25). While relatively good fits with agreeable reliability factors were given with this space group, the geometries of two TiO_6 octahedra were strongly different from one another. Some atomic positions had to be constrained to retain the same geometry of two TiO_6 octahedra that were inverted to each other along the *c* axis and displaced by $\frac{1}{2}$ along the [110] direction. But large isotropic thermal parameters for some oxygen atoms were observed with such constraints. Finally, adoption of space group *P*4/*nmm* (D_{4h}^7) as proposed for a single crystal of $La_{2-x}M_xCuO_4$ (M = Na, K) (20) gave better thermal factors, although powder X-ray diffraction patterns were insufficient to reveal clear visible evidence of the extinctions by glide plane. Corrections for (00l) preferred orientation were made for all phases. In Table 2, some crystallographic data and the final reliability factors are shown. The observed, calculated, and difference profiles for all phases are plotted in Fig. 1. The refined atomic coordinates and isotropic thermal parameters are listed in Table 3. The idealized structure of $NaLaTiO_4$ is illustrated in Fig. 2. This figure shows well that alternate NaO and *Ln*O double layers are arranged with a sequence of $-(NaO)_2-TiO_2-(LaO)_2-TiO_2-$ along the *c* axis. The Ti atoms are displaced out of plane toward the NaO double layers, leading to a considerable distortion of the TiO_2 layers. The corrugation of *Ln*O layers are also observed while the NaO layers are almost flat. A variation of the unit cell parameters as a function of the radius for constituting lanthanide ions is represented in Fig. 3. Although the *c* parameter decreases as the lanthanide ion become smaller, it is interesting that the *a* parameter does not show any decreasing trend. Such a behavior is explained by the remarkable corrugation of *Ln*O layers as shown in Fig. 2. Selected bond lengths and bond angles are compared with those of $Na_2Ln_2Ti_3O_{10}$ in Table 4. There is large difference in length between Ti–O2 and Ti–O3, the difference being smaller as the radius of the lanthanide ion decreases. The O3–Ln–O3 bond angles are much smaller than 180° for the ideal cubic perovskite structure and become larger when the La^{3+} ion is replaced by the smaller Nd^{3+}, Sm^{3+}, and Gd^{3+} ions. Thus, the contraction of the *Ln*O layer which is the main factor determining the *a* parameter is not induced by a decrease in size of constituting Ln^{3+} ions but is compensated by flattening through the increase of the O3–*Ln*–O3 bond angle. This situation is not the case for $Na_2Ln_2Ti_3O_{10}$ in which there is a perovskite slab containing the central *Ln*TiO_3 perovskite layer (22). The Ln^{3+} ions are 12-fold coordinated in this structure but 9-fold coordinated in Na*Ln*TiO_4 with the so-called K_2NiF_4-derivative structure. The bending of the O–Ln–O bond would be more difficult when the coordination number of the Ln^{3+} ion is 12 rather than 9. Indeed, the angles of the O–Ln–O bonds in $Na_2Ln_2Ti_3O_{10}$ are much larger than those of the O3–Ln–O3 bonds in Na*Ln*TiO_4 and show no systematic change (see Table 4). In consequence, the *a* parameter for $Na_2Ln_2Ti_3O_{10}$ gradually decreases when the lathanide ion becomes smaller, indicating that the contraction of the *Ln*TiO_3 layer is not compensated for by a decrease of the O–Ln–O bond bending. The strong corrugation in Na*Ln*TiO_4, therefore, could be correlated to the weak interaction in *Ln*O layer with low coordination number. Such a consideration explains well the facts that, despite the decrease in radius of constituting large cations, the

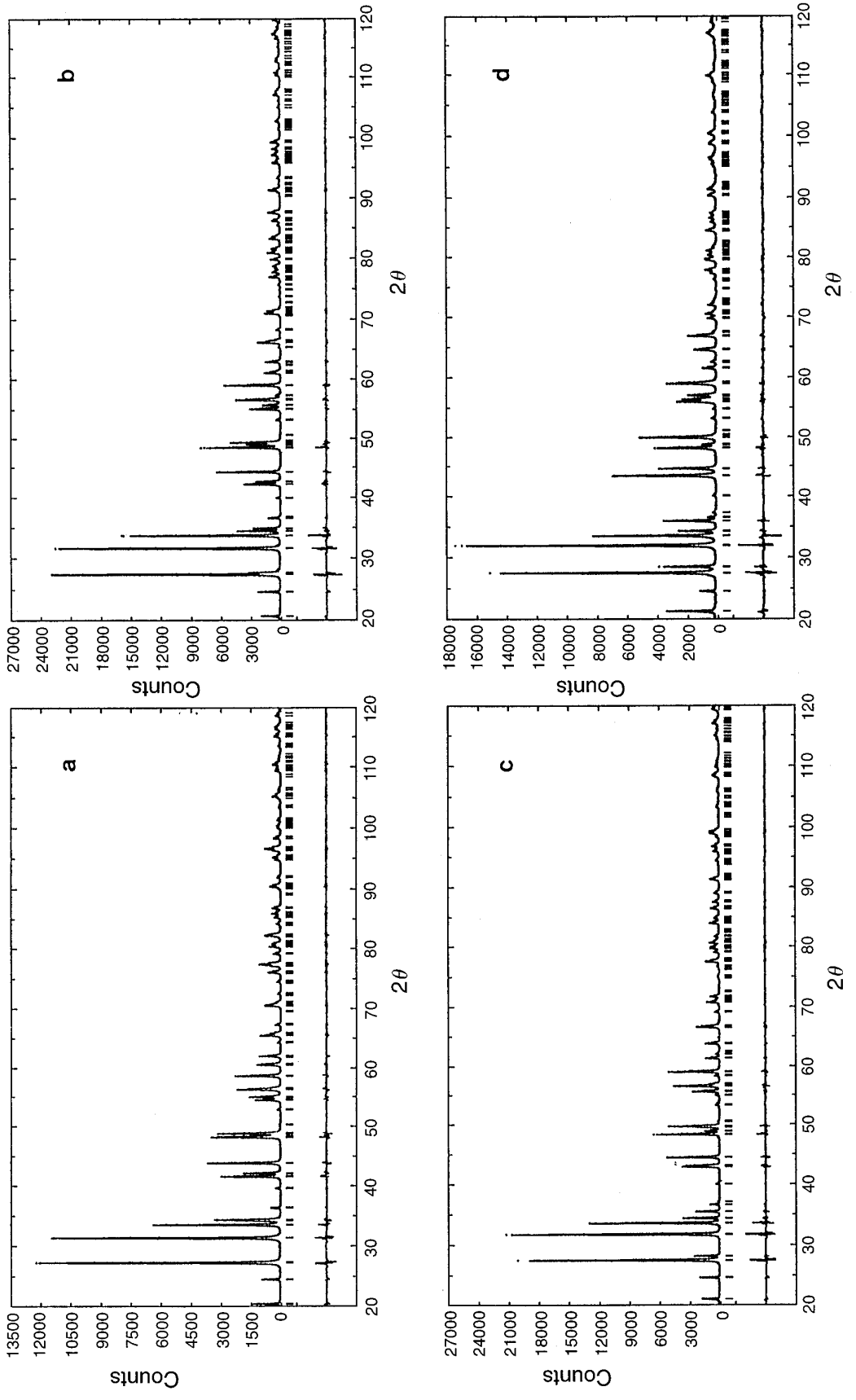

FIG. 1. Calculated (solid line), experimental (dotted line), and difference (solid line on the bottom) X-ray powder diffraction pattern of NaLnTiO$_4$ where Ln = La (a), Nd (b), Sm (c), and Gd (d).

TABLE 3
Atomic Positions and Isotropic Temperature Fators for Na*Ln*TiO$_4$ (*P*4/*nmm* with Second Setting)

	$NaLaTiO_4$	$NaNdTiO_4$	$NaSmTiO_4$	$NaGdTiO_4$
Ln	La	Nd	Sm	Gd
x	0.25	0.25	0.25	0.25
y	0.25	0.25	0.25	0.25
z	0.8891(2)	0.8914(2)	0.8920(3)	0.8922(2)
B(Å^2)	0.57(5)	0.42(6)	0.44(7)	0.42(8)
Na				
x	0.25	0.25	0.25	0.25
y	0.25	0.25	0.25	0.25
z	0.585(1)	0.586(1)	0.588(2)	0.588(2)
B(Å^2)	1.3(5)	1.3(5)	1.3(7)	0.7(7)
Ti				
x	−0.25	−0.25	−0.25	−0.25
y	−0.25	−0.25	−0.25	−0.25
z	0.7246(5)	0.7296(6)	0.7317(7)	0.7344(6)
B(Å^2)	0.50(1)	0.32(5)	0.47(2)	0.44(2)
O(1)				
x	−0.25	−0.25	−0.25	−0.25
y	0.25	0.25	0.25	0.25
z	0.758(1)	0.724(1)	0.766(2)	0.770(1)
B(Å^2)	0.7(3)	0.8(4)	1.4(5)	1.8(6)
O(2)				
x	0.25	0.25	0.25	0.25
y	0.25	0.25	0.25	0.25
z	0.407(2)	0.407(3)	0.403(2)	0.402(2)
B(Å^2)	1.3(5)	0.6(5)	1.3(8)	1.4(7)
O(3)				
x	0.25	0.25	0.25	0.25
y	0.25	0.25	0.25	0.25
z	0.071(2)	0.072(2)	0.070(3)	0.074(3)
B(Å^2)	1.1(5)	0.6(6)	1.9(8)	1.9(9)

constancy or even increasing tendency of the *a* parameter is often observed for structures with two-dimensional character. The O2–Na–O2 angles are much larger than those of O3–La–O3 bonds and a corrugation of the NaO layer, a minor factor in determining the *a* parameter, is very weak.

Ionic Conductivity

Complex impedance plane plots of the imaginary part vs the real part for Na*Ln*TiO$_4$ (*Ln* = La, Nd, Sm, and Gd) was typical semi-circle. The ionic conductivities were obtained using the resistance values determined from the intersection of that semi-circle with the real part axis. Arrhenius plots of ionic conductivities illustrated in Fig. 4 show that these compounds are poor conductors whose conductivities are one order lower than those of $Na_2Ln_2Ti_3O_{10}$. Seeing Table 4, the Na–O2 bonds of Na*Ln*TiO$_4$ shorter than those of $Na_2Ln_2Ti_3O_{10}$ are consistent with lower conductivity. In addition, the conductivity decreases from *Ln* = La to Nd, Sm, and Gd. At first sight, such a decrease in conductivity might be reasonable because the replacement of a La^{3+} ion by Nd^{3+}, Sm^{3+}, and Gd^{3+} will reduce more and more the lattice volume of Na*Ln*TiO$_4$ and decrease the available space for the migration of sodium ions. This point of view may be in agreement with the observations that the lattice contraction resulting from the decrease of constituting ionic size or the application of external hydrostatic pressure leads to the decrease of the ionic conductivity (26, 27). If we compare with the variation of conductivity in $Na_2Ln_2Ti_3O_{10}$ when the Ln^{3+} ions change from La^{3+} to Nd^{3+}, Sm^{3+}, and Gd^{3+} (19), however, that in Na*Ln*TiO$_4$ shows a completely opposite trend. In the case of $Na_2Ln_2Ti_3O_{10}$, the ionic conductivity was observed to increase from *Ln* = La, to Nd, Sm, and Gd.

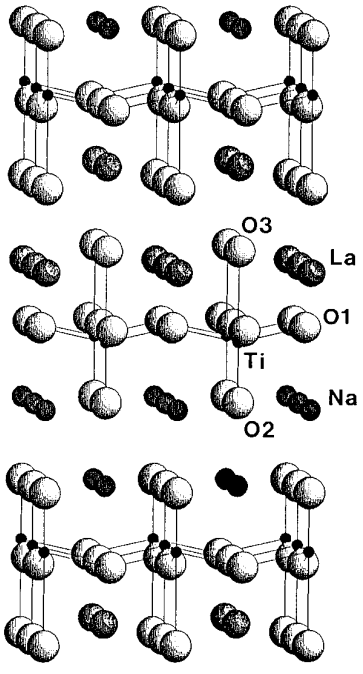

FIG. 2. Schematic view of the structure for $NaLaTiO_4$. Only Ti–O bonds are described by lines. (Na = dark medium size spheres, La = shaded large spheres, Ti = small black spheres, and O = white spheres)

This phenomenon was explained by the fact that the NaO layer is not influenced by a decrease of the *c* parameter, but instead the increased covalency of the perovskite slab by a contraction along the *c* axis gives higher ionic character to the Na–O bond competing with the Ti–O bond of the perovskite slab.

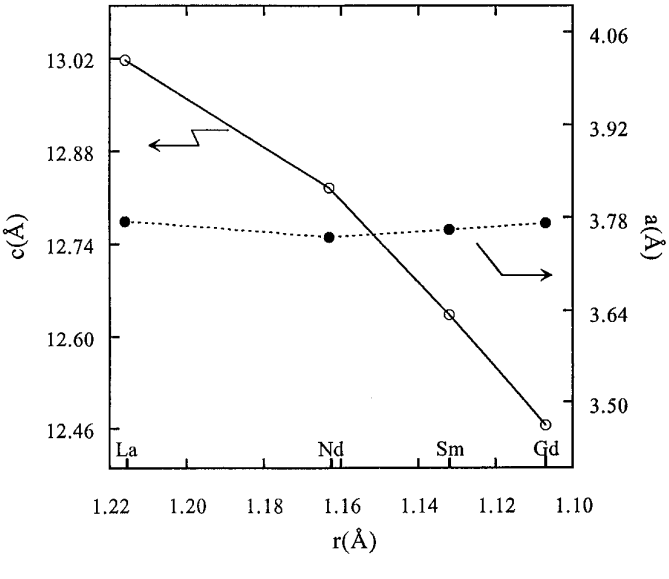

FIG. 3. Variations of the lattice parameters of NaLnTiO$_4$ (Ln = La, Nd, Sm, and Gd) as a function of the radii of lanthanide ions.

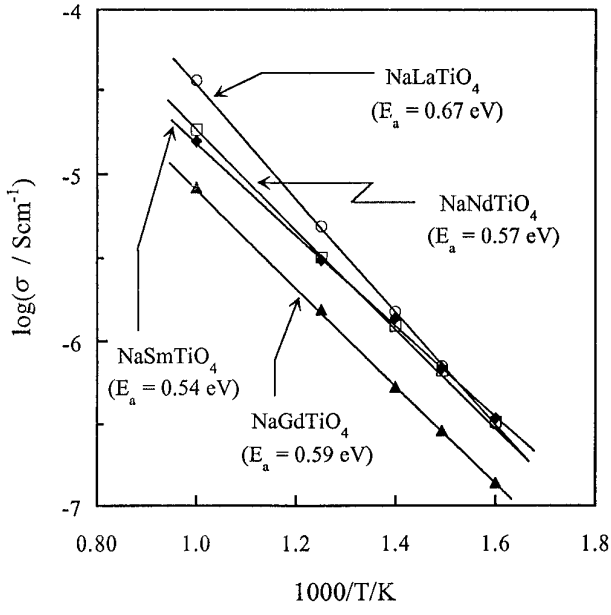

FIG. 4. Plots of log σ vs $1/T$ for NaLnTiO$_4$ (Ln = La, Nd, Sm, and Gd). The activation energies calculated from corresponding slopes are indicated in parentheses.

Such contradicting behavior of similar-layered structures would be understood through a detailed comparison of the two types of structure. First of all, it must be noted again that the change of the Na–O2(x1) bond distance perpendicular to the layer shows an increasing trend or is at least almost constant, although the *c* parameter strongly decreases from Ln = La to Nd, Sm, and Gd. This tendency is quite similar with that of Na–O3(x1) bonds in $Na_2Ln_2Ti_3O_{10}$. In contrast, an important difference could be deduced when we compare the O2–Na–O2 bond angle in NaLnTiO$_4$ with that in $Na_2Ln_2Ti_3O_{10}$. The angle decreases from Ln = La to Gd in $Na_2Ln_2Ti_3O_{10}$, whereas it increases in NaLnTiO$_4$ toward a more stable and regular rock-salt-type NaO layer. It could be concluded, therefore, that the more effective cubic closest packing of the NaO layer is responsible for the decrease in ionic conductivity of NaLnTiO$_4$ from Ln = La to Nd, Sm, and Gd.

CONCLUSION

In the case of $Na_2Ln_2Ti_3O_{10}$, the perovskite slab containing $LnTiO_3$ layers where Ln^{3+} ions are 12-fold coordinated keeps a characteristic feature of three-dimensional perovskite lattice, whereas, in the case of NaLnTiO$_4$, the $Na_{0.5}Ln_{0.5}$ TiO_3 layer where both Na^+ and Ln^{3+} ions are 9-fold coordinated loses a character of typical perovskite lattice. Therefore, a poor charge balance between NaO and LnO layers in NaLnTiO$_4$ can lead to effective corrugation of the LnO layer as well as a considerable shift of

TABLE 4
Selected Bond Lengths (Å) and Bond Angles (°) for Na*Ln*TiO$_4$

	Ln = La	Nd	Sm	Gd
		Bond lengths		
Ti–O1 (× 4)	1.953(3)	1.927(4)	1.931(5)	1.936(5)
Ti–O2 (× 1)	1.72(2)	1.74(3)	1.70(3)	1.71(3)
[Ti2–O3 (× 1)	1.72(4)	1.68(6)	1.63(8)	1.67(7)][a]
Ti–O3 (× 1)	2.66(2)	2.54(3)	2.51(4)	2.39(3)
Na–O2 (× 4)	2.670(1)	2.654(1)	2.662(2)	2.669(2)
[Na–O3 (× 4)	2.7126(3)	2.701(3)	2.692(3)	2.679(2)][a]
Na–O2 (× 1)	2.31(2)	2.30(3)	2.34(3)	2.33(3)
[Na–O3 (× 1)	2.31(5)	2.33(8)	2.42(9)	2.35(8)][a]
Ln–O3 (× 4)	2.719(4)	2.693(4)	2.703(6)	2.699(5)
Ln–O3 (× 1)	2.37(2)	2.32(3)	2.24(3)	2.27(3)
		Bond angles		
O1–Ti–O1 (× 2)	154.3(2)	153.4(2)	153.8(3)	153.8(2)
O2–Na–O2 (× 2)	175.5(3)	176.1(4)	177.1(5)	179.7(5)
[O3–Na–O3 (× 2)	178.9(2)	176.4(4)	175.2(5)	176.4(4)][a]
O3–*Ln*–O3 (× 2)	158.0(2)	159.9(3)	159.5(4)	162.0(3)
[O1–*Ln*–O1 (× 2)	169.8(3)	171.1(5)	174.5(6)	169.8(6)][a]

[a] Bond lengths and bond angles for $Na_2Ln_2Ti_3O_{10}$ (22).

Ti^{4+} ion toward the NaO double layer in order to compensate for it. Based on the difference in variation of ionic conductivity for Na*Ln*TiO$_4$ and $Na_2Ln_2Ti_3O_{10}$, it could be suggested that the ionic conduction in layered perovskite structure is not dependent on the average structure but on the local modification of available sites for mobile ions.

ACKNOWLEDGMENT

This work was supported by the Center for Molecular Catalysis and the Korea Science and Engineering Foundation (941-0300-028-2).

REFERENCES

1. S. N. Ruddlesden and P. Popper, *Acta Crystallogr.* **10,** 538 (1957).
2. M. Dion, M. Ganne, and M. Tournoux, *Mater. Res. Bull.* **16,** 1429 (1981).
3. A. J. Jacobson, J. M. Johnson, and J. T. Lewandowski, *Inorg. Chem.* **24,** 3727 (1985).
4. A. J. Jacobson, J. T. Lewandowski, and J. W. Johnson, *J. Less-Common Met.* **116,** 137 (1986).
5. K. Domen, J. Yoshimura, T. Sekine, A. Tanaka, and T. Onishi, *Catal. Lett.* **4,** 339 (1990).
6. R. A. Mohan Ram and A. Clearfield, *J. Solid State Chem.* **94,** 45 (1991).
7. J. Gopalakrishinan, S. Uma, and V. Bhat, *Chem. Mater.* **5,** 132 (1993).
8. J. Yoshimura, Y. Ebina, J. Kondo, K. Domen, and A. Tanaka, *J. Phys. Chem.* **97,** 1970 (1993).
9. S. Uma and J. Gopalakrishinan, *Chem. Mater.* **6,** 907 (1994).
10. S. H. Byeon, I. S. Kim, M. Itoh, and T. Nakamura, *Mater. Res. Bull.* **28,** 597 (1993).
11. G. Demazeau, J. L. Marty, M. Pouchard, T. Rojo, J. M. Dance, and P. Hagenmuller, *Mater. Res. Bull.* **16,** 47 (1981).
12. R. A. Mohan Ram, K. K. Singh, W. H. Madhusudan, P. Ganguly, and C. N. R. Rao, *Mater. Res. Bull.* **18,** 703 (1983).
13. G. Demazeau, L. M. Zhu, L. Fournes, M. Pouchard, and P. Hagenmuller, *J. Solid State Chem.* **72,** 31 (1988).
14. L. M. Zhu, G. Demazeau, M. Pouchard, J. M. Dance, and P. Hagenmuller, *J. Solid State Chem.* **78,** 46 (1989).
15. S. H. Byeon, G. Demazeau, J. H. Choy, and J. M. Dance, *Eur. J. Solid State Inorg. Chem.* **28,** 643 (1991).
16. S. H. Byeon, G. Demazeau, J. H. Choy, and P. Hagenmuller, *C.R. Acad. Sci. Ser. II* **312,** 37 (1991).
17. G. Demazeau, S. H. Byeon, J. H. Choy, and P. Hagenmuller, *Z. Anorg. Allg. Chem.* **610,** 91 (1992).
18. H. T. Witteveen, Thesis, University of Leyde, 1973.
19. G. Blasse, *J. Inorg. Nucl. Chem.* **30,** 656 (1968).
20. S. L. Stoll, A. M. Stacy, and C. C. Torardi, *Inorg. Chem.* **33,** 2761 (1994).
21. M. Richard, G. Goglio, and L. Brohan, *Mater. Res. Bull.,* **30,** 925 (1995).
22. K. Park and S. H. Byeon, *Bull. Kor. Chem. Soc.,* in press.
23. F. Izumi, H. Murata, and N. Watanabe, *J. Appl. Crystallogr.* **20,** 411 (1987).
24. A. Daoudi, Thesis, University of Bourdeaux I, 1974.
25. G. Blasse and G. P. M. Van den Heuvel, *J. Solid State Chem.* **10,** 206 (1974).
26. M. Itoh, Y. Inaguma, W. H. Jung, L. Chen, and T. Nakamura, *Solid State Ionics* **70/71,** 203 (1994).
27. Y. Inaguma, J. Yu, Y. J. Shan, M. Itoh, and T. Nakamura, *J. Electrochem. Soc.* **142,** L8 (1995).